Bridging Like-Charged Macroions through Long Divalent Rodlike Ions

Sylvio May,[†] Aleš Iglič,[‡] Jurij Reščič,[§] Stefano Maset,[||] and Klemen Bohinc*[,‡,⊥]

Department of Physics, North Dakota State University, Fargo, North Dakota 58105-5566, Faculty of Electrical Engineering, Tržaška 25, University of Ljubljana, 1000 Ljubljana, Slovenia, Faculty of Chemistry and Chemical Technology, University of Ljubljana, 1000 Ljubljana, Slovenia, Dipartimento di Matematica e Informatica, Universita 'di Trieste, 34100 Trieste, Italy, and University College of Health Studies, Poljanska 26a, University of Ljubljana, 1000 Ljubljana, Slovenia

Received: May 2, 2007; In Final Form: October 29, 2007

Like-charged macroions in aqueous electrolyte solution can attract each other because of the presence of inter- and/or intramolecular correlations. Poisson−Boltzmann theory is able to predict attractive interactions if the spatially extended structure (which reflects the presence of intramolecular correlations) of the mobile ions in the electrolyte is accounted for. We demonstrate this for the case of divalent, mobile ions where each ion consists of two individual charges separated by a fixed distance. Variational theory applied to this symmetric 2:2 electrolyte of rodlike ions leads to an integro-differential equation, valid for arbitrary rod length. Numerical solutions reveal the existence of a critical rod length above which electrostatic attraction starts to emerge. This electrostatic attraction is distinct from nonelectrostatic depletion forces. Analysis of the orientational distribution functions suggests a bridging mechanism of the rodlike ions to hold the two macroions together. For sufficiently large rod length, we also observe "overcharging", that is, an over-compensation of the macroion charges by the diffuse layer of mobile rodlike ions. Our results emphasize the importance of the often rodlike internal structure that condensing agents such as polyamines, peptides, or polymer segments exhibit. The results were compared with Monte Carlo simulations.

1. Introduction

Electrostatic interactions between charged macroions in electrolyte solutions are omnipresent in colloid science, cellular biology, and technological applications; an extensive body of studies, both experimental and theoretical, exists.[1] Electrolytes consisting of multivalently charged ions are among the most interesting systems as they are often found to mediate attractive interactions between like-charged macroions. A well-documented example is the condensation of DNA by a multitude of condensing agents such as the polyamines spermine and spermidine, cationic polypeptides or proteins, multivalent metal cations,[2,3] and nanoparticles.[4] Some of these condensing agents can have a variable shape as is the case for cationic amphiphiles or polymers. In addition, they are often able to adjust their charge distribution, even if subjected to the hypothetical constraint of a fixed shape. For example, the lipids in mixed cationic membranes are mobile and thus may optimize their lateral distribution through a diffusive process.[5] On the other hand, in certain cationic polymers such as polyethylenimine (PEI),[6] the local charge density is adjustable via the degree of ionization.[7] Complexation of macroions other than DNA is also frequently observed, examples include network formation in actin solutions[8] and the aggregation of rodlike M13 virus, induced by a divalent tunable diamin ion.[9] As a common feature in almost all cases, the condensing agent is not simply a multivalent pointlike ion but has an internal structure with its individual charges well-separated from each other and with possibly additional internal ionic degrees of freedom.

The observation of attractive interactions between like-charged macroions in aqueous solution has initiated considerable theoretical interest. One reason is that the mean-field level theoretical description, Poisson−Boltzmann theory, does not predict attraction between equally charged surfaces.[10,11] Hence, in order to obtain attraction, correlations need to be included. The fact that interionic correlations, correlations between mobile ions, can lead to attraction was realized early by Kirkwood and Shumaker[12] and Oosawa,[13] later studied by Monte Carlo (MC) simulations,[14] and various other methods.[15−17] A simple interpretation of the mechanism that leads to attraction can be given in the low-temperature limit where condensed counterions form two-dimensional Wigner crystals on the surface of each macroion. Interlocking of the crystals then gives rise to a short-range attractive force. However, Linse has shown that correlation attraction occurs even if no Wigner Crystal arrangement is present.[18] Experimentally observed attractive forces, such as those between like-charged mica or clay surfaces in a solution of divalent ions,[19,20] are in agreement with this interpretation.

Attractive interactions between like-charged macroions can also arise through intra-ionic correlations, that is, correlations between the spatially separated charges of a single multivalent microion. A notable example is the ability of polyelectrolytes to complex oppositely charged macroions[21] as is observed for the condensation of DNA induced by cationic polymers.[22] Direct experimental observations of attractive, polyelectrolyte-induced forces, based on the surface force apparatus, have also been reported.[23] To understand the emergence of attractive interactions in these systems, no correlations between polymers need to be included. That is, a theoretical model on the Poisson−Boltzmann level already produces attractive interactions, given

* Corresponding author. Present address: Department of Physics, North Dakota State University, Fargo, ND 58105-5566.
[†] North Dakota State University.
[‡] Faculty of Electrical Engineering, University of Ljubljana.
[§] Faculty of Chemistry and Chemical Technology, University of Ljubljana.
[||] Universita 'di Trieste.
[⊥] University College of Health Studies.

10.1021/jp073355e CCC: $40.75
Published on Web 01/19/2008

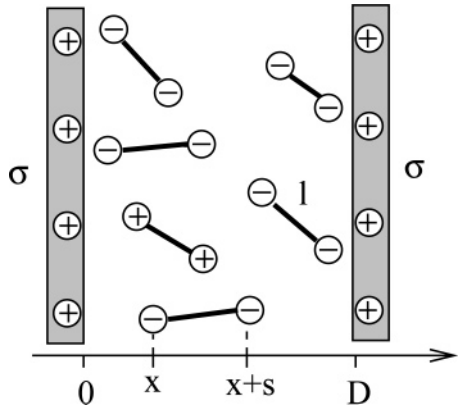

Figure 1. Schematic illustration of two like-charged planar surfaces, located at positions 0 and D along the horizontal axis with σ denoting the corresponding surface charge density. The surfaces are immersed in an electrolyte solution that contains negatively and positively charged rodlike divalent counter- and co-ions. The separation between the individual charges of each rodlike ion is denoted by l. The coordinates x and $x + s$ specify the instantaneous positions of the two charges in a given rodlike ion along the horizontal axis.

that the segment connectivity within the polymer chains (which reflects the presence of intra-ionic correlations within the polyelectrolyte) is accounted.[24−26] Two related physical effects predicted for polyelectrolytes interacting with macroions are overcharging[27,28] and bridging.[29,30] The former implies charge inversion, that is, an accumulation of excess charge above that needed to neutralize the surface charges of the macroions. The latter describes the mechanism of individual polyelectrolytes being adsorbed onto two macroions at the same time. Both effects are intimately connected to the existence of a stable equilibrium distance between the two like-charged macroions.

Perhaps the most simple multivalent ion with a spatially extended charge distribution would consist of two individual point-charges separated by a fixed distance l. This rodlike ion type was the subject of a recent study[31] in which a nonlinear Poisson−Boltzmann equation was derived in the limit of sufficiently small rod length l (resulting from a Taylor expansion and being strictly valid only for $l \ll l_D$, where l_D is the Debye screening length). The possibility of attractive interactions between two like-charged planar macroions was indeed predicted, but only if the rod is longer than a critical value l_c with, generally, $l_c > l_D$. Clearly, because our previous approach was based on small l, the presence of attraction is still questionable. One of our goals is thus to extend our previous approach to arbitrary rod length l and to study if attractive interactions still exist.

In particular, we shall develop the theory for the case of arbitrary long rodlike ions sandwiched between two like-charged planar surfaces. Any correlations between the mobile rodlike ions will be neglected. Yet, the internal structure of each rodlike ion is fully accounted for. Numerical solutions of the resulting integrodifferential equation corroborate the possibility of attractive electrostatic interactions between the two like-charged macroions. In the limit of weak macroion charge density, they emerge for $l > l_c \approx 2l_D$. Below, we shall present an interpretation of the electrostatic attraction in terms of the above-mentioned bridging mechanism.

2. Theory

The system we consider is schematically displayed in Figure 1 and consists of two planar, like-charged surfaces immersed in a symmetric 2:2 electrolyte. The mobile ions residing between the two surfaces are in equilibrium with a bulk reservoir of concentration n_0. The two surfaces, each of area $A = Na$ with N fixed positive charges attached, are parallel and separated by distance D. We note the corresponding (positive) surface charge density $\sigma = e/a$, where e is the elementary charge and a is the cross-sectional area per charge on each planar macroion. Our choice of the planar geometry is guided by simplicity rather than by any particular application; it ensures that all average properties of the system depend only on the normal direction of the macroion's planar surfaces, the x axis. The special feature of our system is the structure of the divalent ions. Instead of having point-like ions, each one consists of two individual charges separated by a fixed distance l. The electrolyte thus contains two structurally equivalent but oppositely charged rodlike ionic species that are free to optimize their spatial distribution and orientations everywhere between the two planar surfaces.

Let us describe the locations and orientations of the positively and negatively charged rodlike ions by the ionic distribution functions $n_+(x, s)$ and $n_-(x, s)$, respectively. We refer to one of the two charges of a rodlike ion as a reference charge. The local concentration of the reference charges for the positively charged rodlike ions is then $n_+(x) = \langle n_+(x, s)\rangle$, where we define the average value

$$\langle g(s)\rangle = \frac{1}{2l}\int_{-l}^{l} \mathrm{d}s\, g(s) \tag{1}$$

of any given function $g(s)$ in the region $-l \le s \le l$. Similarly, the conditional probability density to find the second charge of a positively charged rodlike ion at $x + s$ if the first is located at x is given by $p_+(s|x) = n_+(x, s)/\langle n_+(x, s)\rangle$. Hence, the ionic distribution function appears as the familiar joint probability

$$n_+(x, s) = n_+(x)p_+(s|x) \tag{2}$$

Analogous quantities $n_-(x) = \langle n_-(x, s)\rangle$ and $p_-(s|x) = n_-(x, s)/\langle n_-(x, s)\rangle$ are introduced for the negatively charged rodlike ions.

Let us discuss the free energy of the system. It will contain an expression for the electrostatic energy, a nonelectrostatic potential that accounts for the presence of the walls, and entropy terms (for both ionic species, positively and negatively charged rodlike ions) that describe the translational and orientational degrees of freedom. Within our approach, the translational entropy is simply that of an ideal gas. Concerning the orientational entropy, all ion orientations in the absence of any external potential must have the same probability. Averaging over two spatial coordinates (the y and z direction) then leads to a constant density of states in the region $-l \le s \le l$ along the x axis. Of course, the total orientational space for a single ion with fixed reference charge, namely, the area of a sphere of radius l, is obtained by also averaging over the remaining spatial direction, $2\pi l \int_{-l}^{l} \mathrm{d}s = 4\pi l^2$.

We are now in the position to write down the electrostatic free energy of the system, F, measured in units of the area A and of the thermal energy kT (here k is Boltzmann's constant and T is the absolute temperature). It can be expressed as

$$\frac{F}{AkT} = \int_{-\infty}^{\infty} \mathrm{d}x \left[\frac{\Psi'(x)^2}{8\pi l_B} + \sum_{i=\{+,-\}} \left\langle n_i(x, s)\left(\ln\frac{n_i(x, s)}{n_0} - 1 + U(x, s)\right)\right\rangle + 2n_0\right] \tag{3}$$

where the sum runs over "+" and "−" and where $l_B \approx 0.7$ nm is the Bjerrum length in water. The symbol Ψ denotes the commonly used dimensionless electrostatic potential, and a prime denotes the derivative with respect to the argument. Hence, the first term in eq 3 is the total electrostatic energy of the system. The second term accounts for all nonelectrostatic interactions. It contains, first, the entropy of the rodlike ions

$$S = -k\int_{-\infty}^{\infty} dx \sum_{i=\{+,-\}} \left\langle n_i(x,s)\left(\ln\frac{n_i(x,s)}{n_0} - 1\right)\right\rangle = -k\int_{-\infty}^{\infty} dx \sum_{i=\{+,-\}} n_i(x)\left[\ln\frac{n_i(x)}{n_0} - 1 + \langle p_i(s|x)\ln p_i(s|x)\rangle\right] \quad (4)$$

where the second line is the decomposition into the translational and orientational entropy. (Note that the above-mentioned uniformity of orientational states along the x axis is expressed by the absence of a degeneracy term in the expression for the orientational entropy). It contains, second, an additional potential $U(x, s)$ (expressed in units of kT) that specifies an external nonelectrostatic interaction for a rodlike ion whose two charged ends reside at positions $x_1 = x$ and $x_2 = x + s$. Because of the symmetry of the rodlike ions, the external potential should not distinguish between the two charges. Therefore, we require symmetry of $U(x, s)$ with respect to exchanging the positions $x_1 \rightarrow x_2$ and $x_2 \rightarrow x_1$. This gives rise to the relation $U(x, s) = U(x + s, -s)$. Apart from this symmetry relation, we do, at this point, not need to further specify the external potential. Below we shall define $U(x, s)$ so as to describe the presence of the macroion's planar surfaces.

In thermal equilibrium, the ionic distribution functions $n_+(x, s)$ and $n_-(x, s)$ are free to adjust such that F in eq 3 adopts a minimum. We find the corresponding optimal distributions by performing the first variation of F with respect to $n_+(x, s)$ and $n_-(x, s)$. Using Poisson's equation, $\Psi''(x) = -4\pi l_B\rho(x)/e$, this gives rise to

$$\frac{\delta F}{AkT} = \int_{-\infty}^{\infty} dx\left[\Psi(x)\delta\left(\frac{\rho(x)}{e}\right) + \sum_{i=\{+,-\}}\left\langle \delta n_i(x,s)\left(\ln\frac{n_i(x,s)}{n_0} + U(x,s)\right)\right\rangle\right] \quad (5)$$

The local charge density, appearing in Poisson's equation and in eq 5,

$$\rho(x) = e\sum_{i=\{+,-\}} i\langle n_i(x,s) + n_i(x-s,s)\rangle + \rho_{fix}(x) \quad (6)$$

accounts for both individual charges of positively ($i = +$) and negatively charged ($i = -$) rodlike ions that make a contribution at position x. That is, the local charge density has contributions from the reference charges that are located at x (first term in the sum in eq 6) and from the second, orientationally mobile, charges (second term in the sum in eq 6) of the rodlike ions. We have also included into $\rho(x)$ an additional fixed charge density $\rho_{fix}(x)$ which is independent of $n_+(x, s)$ and $n_-(x, s)$. At this point, we need not specify $\rho_{fix}(x)$; below, we shall use it to describe the fixed charges on the macroion's planar surfaces.

To carry out the variation $\delta\rho(x)$ in eq 5, we note the equality

$$\int_{-\infty}^{\infty} dx\langle\Psi(x)\delta n_i(x-s,s)\rangle = \int_{-\infty}^{\infty} dx\langle\Psi(x+s)\delta n_i(x,s)\rangle \quad (7)$$

valid for both $i = +$ and $i = -$. With this, the final result for the variation becomes

$$\frac{\delta F}{AkT} = \int_{-\infty}^{\infty} dx \sum_{i=\{+,-\}} \langle\delta n_i(x,s)(i\Psi(x) + i\Psi(x+s) \quad (8)$$

$$+ \ln\frac{n_i(x,s)}{n_0} + U(x,s))\rangle \quad (9)$$

Hence, in thermal equilibrium, the optimal ionic distribution functions are

$$n_i(x,s) = n_0\, e^{-i[\Psi(x)+\Psi(x+s)]-U(x,s)} \quad (10)$$

with $i = +$ and $i = -$. Once the $n_i(x, s)$ are known, we can calculate the local concentrations and the conditional probability densities defined above, yielding

$$n_i(x) = \langle n_i(x,s)\rangle = n_0\langle e^{-i[\Psi(x)+\Psi(x+s)]-U(x,s)}\rangle$$

$$p_i(s|x) = \frac{n_i(x,s)}{\langle n_i(x,s)\rangle} = \frac{e^{-i\Psi(x+s)-U(x,s)}}{\langle e^{-i\Psi(x+s)-U(x,s)}\rangle} \quad (11)$$

Moreover, upon inserting $n_i(x, s)$ into eq 6, we can calculate the charge density

$$\rho(x) = \rho_{fix}(x) + e\sum_{i=\{+,-\}} in_0\langle e^{-i[\Psi(x)+\Psi(x+s)]-U(x,s)} + e^{-i[\Psi(x-s)+\Psi(x)]-U(x-s,s)}\rangle \quad (12)$$

Replacing s with $-s$ in the last term of eq 12

$$\langle e^{-i[\Psi(x)+\Psi(x-s)]-U(x-s,s)}\rangle = \langle e^{-i[\Psi(x)+\Psi(x+s)]-U(x+s,-s)}\rangle \quad (13)$$

and recalling $U(x + s, -s) = U(x, s)$ on the right-hand side of eq 13, we obtain the final expression for the charge density

$$\rho(x) = -4en_0\langle e^{-U(x,s)}\sinh[\Psi(x) + \Psi(x+s)]\rangle + \rho_{fix}(x) \quad (14)$$

Using this expression for $\rho(x)$ in Poisson's equation yields the nonlinear integrodifferential equation

$$2\Psi''(x) = \kappa^2\langle e^{-U(x,s)}\sinh[\Psi(x) + \Psi(x+s)]\rangle - 8\pi l_B\frac{\rho_{fix}(x)}{e} \quad (15)$$

where we have defined the Debye length $l_D = 1/\kappa$ through $\kappa^2 = 4 \times 8\pi l_B n_0$. This definition of the Debye length is equivalent to that of a symmetric 2:2 electrolyte containing divalent pointlike ions. Inserting the equilibrium distributions for $n_+(x, s)$ and $n_-(x, s)$ into the free energy in eq 3, we obtain

$$\frac{F}{AkT} = 2n_0\int_{-\infty}^{\infty} dx\langle e^{-U(x,s)}[\Psi(x+s)\sinh[\Psi(x) + \Psi(x+s)] - \cosh[\Psi(x) + \Psi(x+s)]] + 1\rangle + \frac{1}{2}\int_{-\infty}^{\infty} dx\,\Psi(x)\frac{\rho_{fix}(x)}{e} \quad (16)$$

Equation 15, together with the corresponding result for the free energy, eq 16, are major results of the present work, valid for any choice of $U(x, s)$ and $\rho_{fix}(x)$. For our specific system of two charged planar surfaces, located at positions $x = 0$ and $x = D$, we may now specify these functions,

$$U(x, s) = \begin{cases} 0 & x > 0 \;\&\; x + s > 0 \;\&\; x < D \;\&\; x + s < D \\ \infty & \text{elsewhere} \end{cases} \quad (17)$$

and $\rho_{\text{fix}}(x) = \sigma[\delta(x) + \delta(x - D)]$, where we recall $\sigma = e/a$ to be the surface charge density of the two planar surfaces; $\delta(x)$ is the delta function, and a is the cross-sectional area per charge on each surface. Equation 15 then gives the integrodifferential equation

$$2\Psi''(x) = \kappa^2 \frac{1}{2l} \int_{-\min(l,x)}^{\min(l,D-x)} \mathrm{d}s \, \sinh[\Psi(x) + \Psi(x + s)] \quad (18)$$

Note that eq 15 also yields the boundary conditions

$$\Psi'(0) = -\Psi'(D) = -2\kappa p \quad (19)$$

where we have defined the dimensionless measure $p = 2\pi l_B l_D/a$ for the charge density of the macroion surfaces. With our particular choices for $U(x, s)$ and $\rho_{\text{fix}}(x)$, the free energy in eq 16 reads

$$\frac{F}{AkT} = \frac{\Psi(0)}{a} + 2n_0 \int_0^D \mathrm{d}x \Big\{ 1 + \frac{1}{2l} \int_{-\min(l,x)}^{\min(l,D-x)} \mathrm{d}s [\Psi(x + s) \times \sinh[\Psi(x) + \Psi(x + s)] - \cosh[\Psi(x) + \Psi(x + s)]] \Big\} \quad (20)$$

In the present work, we will also consider the linear regime, applicable in the limit $\Psi \ll 1$. In this case, we obtain the linearized integrodifferential equation

$$2\Psi''(x) = \kappa^2 \frac{1}{2l} \int_{-\min(l,x)}^{\min(l,D-x)} \mathrm{d}s [\Psi(x) + \Psi(x + s)] \quad (21)$$

and the free energy, F (see eq 20), reduces to

$$\frac{F}{AkT} = \frac{\Psi(0)}{a} + 2n_0 \int_0^D \mathrm{d}x \Big[1 - \frac{1}{2l} \int_{-\min(l,x)}^{\min(l,D-x)} \mathrm{d}s \Big] \quad (22)$$

The first term on the rhs of eq 22 is the electrostatic contribution to the free energy. Obtaining the surface potential, $\Psi(0)$, involves solving the linearized integrodifferential equation, eq 21. The second term on the rhs of eq 22 is of nonelectrostatic origin and represents the steric depletion interaction due to entropic confinement of the rodlike molecules between the rigid walls. The corresponding integration can be carried out, yielding

$$\int_0^D \mathrm{d}x \Big[1 - \frac{1}{2l} \int_{-\min(l,x)}^{\min(l,D-x)} \mathrm{d}s \Big] = \min(l,D) \Big[1 - \frac{\min(l,D)}{2l} \Big] \quad (23)$$

For $D > l$, eq 23 gives the constant $l/2$, while for $D < l$, eq 23 gives $-D^2/(2l) + D$. In the latter case, the integral in eq 23 decreases quadratically for decreasing D and approaches 0 for $D \to 0$; see curve g in Figure 3B. Note that the simple expression for the depletion energy, based on neglecting all intermolecular steric interactions, is strictly valid only in the dilute regime.

The linearized case has a well-known closed solution in the limit of vanishing length, l, of the rodlike ions. This limit corresponds to pointlike divalent ions for which the linearized integrodifferential equation reads $\Psi''(x) = \kappa^2\Psi(x)$, implying (with boundary conditions given in eq 19) the solution

$$\Psi(x) = 2p \frac{\cosh[\kappa(x - D/2)]}{\sinh(\kappa D/2)} \quad (24)$$

and the corresponding free energy reads

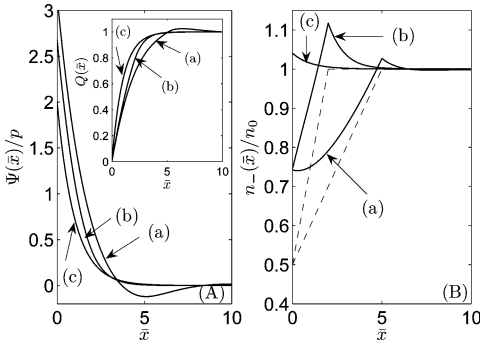

Figure 2. Results for the linearized theory (see eq 21), derived for $p = 0.1$, and large distance $\bar{D} = 20$ between the two surfaces. A: Electrostatic potential $\Psi(\bar{x})/p$ as a function of the distance $\bar{x}$ from the charged surface. The inset shows the scaled integrated charge according to eq 26. B: Local concentration of reference charges $n_-(\bar{x})/n_0$ as a function of $\bar{x}$. Dashed lines display corresponding calculations where electrostatics is excluded ($p = 0$). In all diagrams, the different curves correspond to $\bar{l} = 5$ (a), $\bar{l} = 2$ (b), and $\bar{l} = 0$ (c).

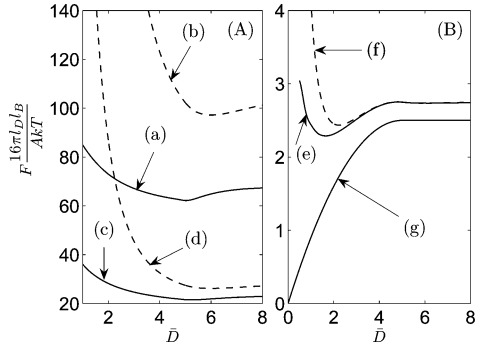

Figure 3. Scaled free energy F as a function of the distance between the two charged planar surfaces, $\bar{D}$, for $\bar{l} = 5$. In both diagrams, the solid curves are derived using nonlinear theory, while the dashed curves are based on linearized theory. The charge parameters correspond to $p = 2$ (a, b), $p = 1$ (c, d), and $p = 0.1$ (e, f). Finally, for curve g, it is $p = 0$, and no electrostatic interactions are present.

$$\frac{F}{AkT} = \frac{\Psi(0)}{a} = \frac{2p}{a} \coth(\kappa D/2) \quad (25)$$

Clearly, for pointlike ions, the interaction energy between the two like-charged surfaces is repulsive. This is also the case in the nonlinear regime.

3. Results

The following analysis is based on numerical solutions of either the nonlinear (see eq 18) or the linearized (see eq 21) integrodifferential equation. The method of solving these integrodifferential equations is outlined in the Appendix; for an isolated surface, an approximate analytical solution is also known.[32] It is convenient to present our results in terms of reduced, dimensionless, spatial coordinates, scaled by the Debye length l_D. Hence, we define $\bar{x} = x/l_D$, $\bar{D} = D/l_D$, $\bar{l} = l/l_D$, $\bar{s} = s/l_D$, and so forth.

Let us first consider the linear regime (see eq 21) at large separation, $\bar{D} = 20$, between the two charged planar surfaces. Figure 2A shows the reduced electrostatic potential $\Psi(\bar{x})/p$ as a function of the distance $\bar{x}$ away from the macroion. The different curves correspond to different rod length $\bar{l}$. Plotting $\Psi(\bar{x})/p$ is convenient because $\Psi(\bar{x}) \sim p$ in the linear regime. Clearly, for $\bar{l} = 0$ the potential is given by eq 24. Note that the potential increases more rapidly for nonvanishing $\bar{l}$ than for $\bar{l} = 0$, which is in agreement with the previous findings[33] for a

single planar macroion (corresponding to $\bar{D} \to \infty$). Upon increasing $\bar{l}$ beyond $\bar{l} > \bar{l}_c \approx 2$, the potential develops nonmonotonic behavior. This behavior directly implies "overcharged" regions where the charges from the rodlike ions overcompensate the macroion charge density at a certain distance away from the macroion. This conclusion follows from the scaled integrated charge (charge per unit area) at distance $\bar{x}$,

$$Q(\bar{x}) = -\frac{l_D}{\sigma}\int_0^{\bar{x}} \rho(\bar{\bar{x}})\, d\bar{\bar{x}} \tag{26}$$

which generally adopts the values $Q(0) = 0$ and $Q(\bar{D}/2) = 1$. In addition, $Q(\bar{x}) > 1$ signifies "overcharging". Rewriting $Q(\bar{x}) = 1 + \Psi'(\bar{x})/(2p)$ we see that regions with $\Psi'(\bar{x}) > 0$ imply $Q(\bar{x}) > 1$. The inset of Figure 2A displays $Q(\bar{x})$ corroborating "overcharging" for $\bar{l} \gtrsim 2$. Note that for $\bar{l} \gtrsim 2$, there is no critical charge parameter p at which the overcharging first appears.

Even though the potential $\Psi(\bar{x})$ in Figure 2A is smooth, the corresponding ionic densities $n_\pm(\bar{x})$ (see eq 11) are not. That this is so for any $\bar{l} > 0$ can be seen directly in the limit of $p = 0$ where no electrostatic interactions are relevant any more; $\Psi \equiv 0$ and $n_+(\bar{x}) = n_-(\bar{x})$. The steric interactions of the rodlike ions still lead to a depletion from the macroions; for $\bar{D} > 2\bar{l}$ the densities are $n_\pm(\bar{x})/n_0 = (1 + \bar{x}/\bar{l})/2$ for $0 \le \bar{x} \le \bar{l}$ and $n_\pm(\bar{x})/n_0 = 1$ for $\bar{l} \le \bar{x} \le \bar{D}/2$. These functions are plotted in Figure 2B (dashed curves, for different rod lengths $\bar{l}$) together with the corresponding results (solid curves) for $n_-(\bar{x})$ in the presence of electrostatic interactions (that is, for $p = 0.1$ as in Figure 2A). Again, the different curves a, b, and c correspond to different rod lengths $\bar{l}$.

Knowing $\Psi(\bar{x})$ allows us to calculate the free energy F (eq 20 in the nonlinear regime and eq 22 in the linear case). Figure 3 shows results for a characteristic case of long ions; $\bar{l} = 5$. Note that, in Figure 3, the scaled free energy $F \times 16\pi l_B l_D/(AkT) = F/(AkT2n_0 l_D)$ is displayed, normalized so as to simply produce the result in eq 23 in the limit $p = 0$ where electrostatic interactions are irrelevant; see curve g in Figure 3. Thus, in this limit ($p = 0$) and for $\bar{D} > \bar{l}$, we find $F \times 16\pi l_B l_D/(AkT) = \bar{l}/2$, (or, equivalently, $F/(AkT) = ln_0$), indicating that the two flat surfaces no longer interact with each other. For small distances, $\bar{D} < \bar{l}$, there is entropy loss of the mobile rods because of their interaction with both surfaces. The corresponding depletion attraction continues to dominate the system for weakly charged surfaces where $p \ll 1$, leading to a minimum in $F(\bar{D})$ at small $\bar{D} < \bar{l}$. For larger surface charge density, $p \gtrsim 1$, a depletion minimum is absent. A second minimum, located roughly at $\bar{D} \approx \bar{l}$, is weak for $p \ll 1$ but dominates the system for $p \gtrsim 1$. This second minimum is distinct from the depletion minimum; it is electrostatic in origin and can be ascribed to a bridging mechanism as analyzed below (see Figure 5). In support of this notion, the bridging minimum occurs for highly charged surfaces almost exactly at $\bar{D} = \bar{l}$; see curve a in Figure 3. The linearized integrodifferential equation (see the dashed curves in Figure 3) makes, qualitatively, the same predictions as the full, nonlinear theory (see the solid curves in Figure 3). Yet, as for pointlike mobile ions, the free energies of the former are much larger if $p \gtrsim 1$.

Similar considerations as for $\bar{l} = 5$ (on which Figure 3 is based) apply to different rod length $\bar{l}$. Our numerical results are summarized in Figure 4 which shows the positions $\bar{D} = \bar{D}_{eq}$ where $F(\bar{D})$ exhibits an absolute minimum. These positions are shown as a function of $\bar{l}$ for different choices of p. Consider first the limit of weakly charged macroions with $p = 0.1$; see curve a in Figure 4. As pointed out above, for sufficiently large

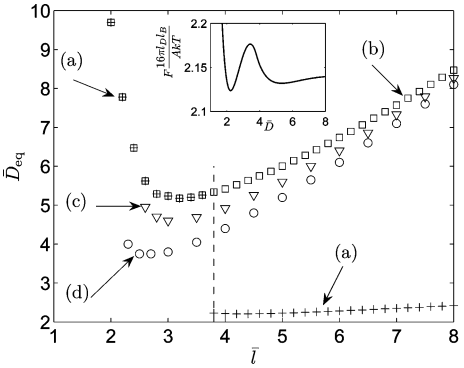

Figure 4. Stable equilibrium distances between the charged surfaces $\bar{D}_{eq}$ as a function of $\bar{l}$. The scaled macroion charge densities are $p = 0.1$ (a), $p = 0.5$ (b, c), and $p = 1$ (d). Curves a and b are derived using linearized theory; for curves c and d, we have used the nonlinear version. Note that the smallest rod length that allows for attraction is $\bar{l} = \bar{l}_c \approx 2$. Note also that, for curve a, the position of the stable minimum jumps at $\bar{l} \approx 3.8$, indicated by the vertical dashed line. The inset shows the corresponding (for $\bar{l} = 3.8$ and $p = 0.1$) scaled free energy as a function of the distance $\bar{D}$ between the charged planar surfaces.

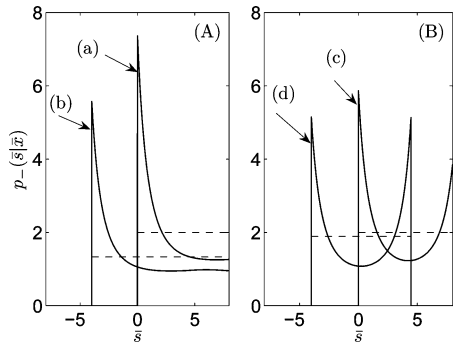

Figure 5. Conditional probability density $p_-(\bar{s}|\bar{x})$ as a function of the projection $\bar{s}$ of the rodlike ions with respect to the $\bar{x}$ axis for two different coordinates of the reference charge; $\bar{x} = 0$ for curves a and c, and $\bar{x} = 4$ for curves b and d. The length of the divalent rodlike ion is $\bar{l} = 8$, and the scaled surface charge density is $p = 0.5$. The dashed lines show corresponding calculations with excluded electrostatics ($p = 0$). The distance between the charged walls is $\bar{D} = 20$ in diagram A, and $\bar{D} = 8.47$ in diagram B.

$\bar{l}$, we observe two local minima, one reflecting the interplay between depletion attraction and electrostatic repulsion and the other one corresponding to an electrostatic bridging mechanism. The bridging minimum is the stable one for sufficiently small $\bar{l}$, namely, for $\bar{l} \lesssim 3.8$. The stable minimum reflecting the interplay between depletion attraction and electrostatic repulsion is adopted for $\bar{l} \gtrsim 3.8$ (see curve a in Figure 4). The position where the two minima exhibit the same depth is at about $\bar{l} \approx 3.8$. This is indicated in Figure 4 by the vertical broken line; the corresponding scaled free energy for $\bar{l} \approx 3.8$ is shown in the inset of Figure 4. Position and depth of the depletion minimum depend on p; for $p = 0.1$ we obtain an equilibrium separation $\bar{D}_{eq} \approx 2.3$; see curve a in Figure 4. Upon an increase of p (with $p \ll 1$), this position shifts to larger $\bar{l}$. For $p \gtrsim 0.5$, only the bridging minimum is left; see curve b in Figure 4.

The location of the bridging minimum is the more interesting one because within linearized theory it is independent of p. Curve b in Figure 4 shows it for $p = 0.5$ where no stable depletion equilibrium is found anymore. (The position of the local bridging minimum for $p = 0.1$ and $\bar{l} \gtrsim 3.8$ is not shown; it would coincide with curve b). For $p = 0.5$, the free energies in linear and nonlinear theory are still fairly close as is evident from the proximity of curves b and c in Figure 4. Curve b of

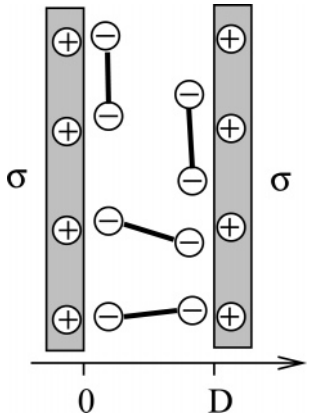

Figure 6. Schematic illustration of the bridging mechanism. For long rodlike ions, $\bar{l} \gg 1$, there exists a stable equilibrium between the two macroions at $\bar{D} \approx \bar{l}$. Here, the ions preferentially orient either parallel or normal to the macroion surfaces. Those aligning normal give rise to the bridging equilibrium.

Figure 4 is a major result of the present study. Its qualitative features are identical to those derived in a previous work[31] where rodlike ions were considered in the limit $\bar{l} \ll 1$, leading to the prediction of attraction for $\bar{l} > \bar{l}_c = 2.45$ (see the inset in the right diagram of Figure 2 in Bohinc et al.[31]). Our present approach, being valid for arbitrary $\bar{l}$, results in the numerically somewhat different prediction $\bar{l}_c \gtrsim 2$. Another similar feature is $\bar{D}_{eq} = \bar{l}$ for $\bar{l} \gg 1$, motivating the interpretation of this minimum to originate in a bridging mechanism.

Increasing the surface charge density ultimately renders the system nonlinear, and the locations, $\bar{D}_{eq} = \bar{D}_{eq}(\bar{l})$, of the bridging minimum will depend on p. Curves b and c in Figure 4, both derived for $p = 0.5$ using the linear and nonlinear approaches, respectively, exhibit the same behavior, $\bar{D}_{eq} = \bar{l}$, for $\bar{l} \gg 1$. They also roughly predict a minimal length $\bar{l}_c = 2$ needed for attractive electrostatic interactions to occur.

Our final analysis characterizes bridging of the rodlike ions as the mechanism that leads to the stable minimum between the like-charged surfaces at $\bar{D}_{eq} \approx \bar{l}$. To this end, we consider the conditional probability density $p_-(\bar{s}|\bar{x})$ (see eq 11) that directly reflects the orientational distribution of the rodlike counterions. As everywhere in this section, $p_-(\bar{s}|\bar{x})$ is expressed in terms of the rescaled coordinates $\bar{x} = x/l_D$ and $\bar{s} = s/l_D$; the normalization condition then reads

$$\frac{1}{2\bar{l}} \int_{-\bar{l}}^{\bar{l}} p_-(\bar{s}|\bar{x})\, d\bar{s} = 1 \qquad (27)$$

valid for $\bar{x}$ in the region $0 \le \bar{x} \le \bar{D}$. For all $\bar{s}$ outside that region, it is $p_-(\bar{s}|\bar{x}) \equiv 0$. Figure 5 shows $p_-(\bar{s}|\bar{x})$ at large $\bar{l}$ for two different cases, large $\bar{D}$ (with $\bar{D} \gg \bar{l} \gg 1$) corresponding to an isolated macroion and $\bar{D} = \bar{D}_{eq} \approx \bar{l}$ where the rodlike ions bridge between the two planar macroions (see Figure 6). In Figure 5, we have specifically chosen $p = 0.5$ and $\bar{l} = 8$, as well as $\bar{D} = 20$ (see diagram A) and $\bar{D} = 8.47$ (see diagram B). In the latter case, $\bar{D} = \bar{D}_{eq}$; see Figure 4. In both diagrams, we display $p_-(\bar{s}|\bar{x})$ for the two positions $\bar{x} = 0$ and $\bar{x} = \bar{l}/2 = 4$.

For $\bar{D} = 20$ (see diagram A of Figure 5), we observe an enhanced probability to find the second charge of the rodlike ion close to the macroion surface, irrespective of whether the first is located at $\bar{x} = 0$ or $\bar{x} = 4$. Clearly then, the rodlike ions exhibit a tendency to align parallel to the macroions' surface.

For $\bar{D} = 8.47$ (see diagram B of Figure 5), there are two regions of enhanced probability density $p_-(\bar{s}|\bar{x})$, corresponding to the location of the rodlike ion's second charge close to either one of the macroion surfaces. Again, this observation applies for both locations of the reference charge at $\bar{x} = 0$ or $\bar{x} = 4$. Hence, our finding is that two different orientations are preferred, with the rodlike ion either parallel or normal to the macroions. It is the latter case that signifies the bridging transition. We thus redisplay, in Figure 6, the schematic representation in Figure 1 for the case of $\bar{D} = \bar{D}_{eq} = \bar{l}$, highlighting the preferred parallel and normal orientations of the rodlike ions. We note that the orientational ordering is induced by electrostatics. For uncharged surfaces, corresponding to $p = 0$, the probability distribution, $p_-(\bar{s}|\bar{x})$, is uniform as shown in Figure 5 (broken lines). In the opposite case, for strongly charged surfaces, with $p \gtrsim 1$, the variations in $p_-(\bar{s}|\bar{x})$ are much stronger than those displayed in Figure 5 (results not shown).

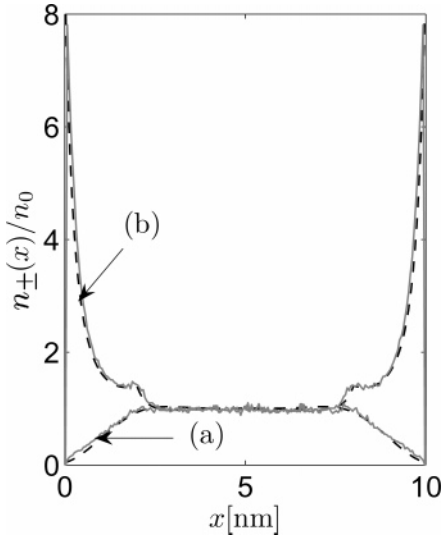

Figure 7. Local concentration of reference charges $n_\pm(x)$ as a function of x. Curve (a) refers to positively charged rodlike ions, and curve (b) refers to negatively charged rodlike ions. Dashed lines display the theoretical approach, whereas full lines display results of MC simulation. The model parameters are: the length of the rodlike ions $l = 2$ nm, their bulk concentration $n_0 = 0.1$ mol/L, the charge parameter $p = 1$ and the plate-to-plate separation $D = 10$ nm. In MC simulations, both ion types are modeled as two charged hard spheres of radius 0.05 nm (separated by the fixed distance l).

We also discuss the probability density distribution of coions and their contribution to the interaction between equally charged surfaces. First note that the concentration of coions is much smaller than the concentration of counterions. In the case $\bar{D} \approx \bar{l}$, $p = 0.5$ and $\bar{l} = 8$ the concentration of counterions close to the charged surface is $n_-(x = 0)/n_0 \approx 3.88$, while the concentration of coions close to the charged surface is $n_+(x = 0)/n_0 \approx 0.07$. With increasing surface charge density the concentration of coions becomes negligibly small compared with the concentration of counterions. This means that the coions have a very small influence on the attraction between equally charged surfaces. In the case of $\bar{D} \approx \bar{l}$, the most probable location of the second charge of the coions is in the midplane of the system regardless of the position of the reference charge.

Our approach accounts for intra-ionic correlations, that is, correlations between the two charges within a given rodlike ion. But it neglects inter-ionic correlations, that is, correlations between charges of different rodlike ions. As is well-known, interionic correlations can be neglected for monolvalent salt solutions (of reasonably low densities). But they become important for pointlike divalent ions. We thus expect our approach to work better for long rodlike ions where the two

charges of each ion are spatially separated so that the electrolyte behaves effectively similar to a monovalent salt. For vanishingly small l, the charges merge into one divalent pointlike ion. Then, correlations between these ions tend to be strong and our approach fails. This notion is supported by Monte Carlo simulations that we have carried out (as described in section 4). We finally note that our approach predicts overcharging independently of the macroion's surface charge density. This is qualitatively different for multivalent pointlike ions where overcharging is a function of the ion radius and involves a critical surface charge density[34,35] (which has been suggested to diverge with decreasing ion radius[36]). The situation considered in the present work is qualitatively different because intra- (instead of inter-) molecular correlations lead to the overcharging.

4. Comparison with Monte Carlo Simulations

Canonical Monte Carlo (MC) simulations were performed using the integrated Monte Carlo/molecular dynamic/Brownian dynamic simulation suite Molsim[37] following the standard Metropolis scheme. Both positive and negative rod-like ions were placed randomly into the Monte Carlo simulation box. The MC box was made electroneutral and average concentrations of both positive and negative charges exactly matched those obtained from the PB calculations. A trial move consists of both random displacement and random rotation. Displacement parameters were chosen to obtain approximately 50% acceptance rate. Thirty thousand attempted moves per particle were used for equilibration followed by 100 000 attempted moves during production runs. Interparticle interactions were calculated as described elsewhere.[38] To calculate single particle distributions, the z axis was divided into 200 bins of width 0.05 nm. The standard deviation of values in histograms was less than 0.5% for each separate bin in all cases. Because the MC simulations cannot be performed using a mixture of pointlike positive and pointlike negative charges, we modeled both ion types as charged hard spheres of radius of 0.05 nm. A small but inevitable difference of the density profiles in the vicinity of charged walls arose due to finite ionic radii.

The comparison between the Monte Carlo simulations and the theory shows that for sufficiently long divalent rodlike ions (in our case $l = 2$ nm) there is a good agreement for the concentration profile of reference charges $n_{\pm}(x)$ (Figure 7). Also the noncontinuous derivatives of $n_{\pm}(x)$ (the concentration of the reference charges) at the positions $x = l$ and $x = D - l$ obtained in the theory is reproduced by our MC simulations. But in the limit of small divalent ions, there is a large discrepancy between our theory and Monte Carlo simulations (not shown).

Our comparison clearly suggests the usefulness of the theory in the limit of long divalent rodlike ions. It also suggests that the overcharging for fixed length of divalent rodlike ions is present for any parameter p. In other words, we did not find a critical surface charge density at which overcharging first appears. Hence, for sufficiently long divalent rodlike ions, the attraction between equally charge surfaces is present for any surface charge density.

5. Conclusion

In summary, we have developed a density functional theory for rodlike ions of arbitrary length, l, subject to an additional nonelectrostatic external potential. The specific application to the case of two interacting, like-charged, planar macroions reveals the possibility of attractive interactions, introduced entirely by correlations within the rodlike ions, rather than between them (the latter being neglected in the mean-field Poisson−Boltzmann approach). Our results qualitatively corroborate previous findings on the interactions induced by rodlike ions that were based on a Taylor expansion with respect to the rod length.[31] Specifically, there is a minimal rod length, l_c, above which the electrostatic interactions can be attractive. In our present approach, this minimal rod length, $l_c \approx 2l_D$, is roughly given by twice the Debye length, l_D, that characterizes the electrostatic screening length. In the limit of large rod length, $l \gg l_D$, an optimal distance, $D \approx l$, between the macroions results from a bridging interaction. We expect that our present results contribute to better understand the often rodlike structure of common condensing agents such as polyamines and certain linear peptides that are able to condense DNA[2,39] and other macroions.[40]

Acknowledgment. Financial support of S.M. from NSF through Grant NSF DMR-0605883 is acknowledged. K.B. and A.I. thank Slovenian Research Agency Grants P2-0232, J3-9219 and BI−US/06-07. J.R. thanks Slovenian Research Agency, Research Project J1-6653. The authors thank Prof. B. Joensson for the helpful discussion.

Appendix

Analytical solution of the integrodifferential eq 18 with boundary conditions (eq 19) is not available in a closed form. A numerical solution is obtained in the following way. The integrodifferential boundary value problem (eqs 18 and 19) is restated as a fixed point equation

$$\Psi = \mathcal{T}(\Psi) \tag{28}$$

where $\mathcal{T}(\Psi)$ is the solution Y of the ordinary differential boundary value problem

$$2\mathrm{Y}''(x) = \kappa^2 \frac{1}{2l} \int_{-\min[l,x]}^{\min[l,D-x]} \mathrm{d}s \, \sinh[\mathrm{Y}(x) + \Psi(x+s)] \tag{29}$$

with boundary conditions $\mathrm{Y}'(x = 0) = -\mathrm{Y}'(x = D) = 4\pi l_B/a$. The fixed point eq 28 is then discretized by replacing the domain $[0, D]$ of eq 18 by a mesh

$$\Omega_N = \{\theta_{N,i}:\ i = 1, ..., N\}$$

$$\theta_{N,i} = \frac{D}{2} + \frac{D}{2} \cos\left(\frac{2i-1}{2N}\pi\right)$$

of N Chebyshev nodes, the function Ψ by an N-dimensional vector Ψ_N of values at the mesh nodes, and eq 28 by the finite dimensional algebraic equation

$$\Psi_N = \pi_N(\mathcal{T}(p_N(\Psi_N))) \tag{30}$$

where $p_N(\Psi_N)$ is the polynomial interpolating the values in the vector Ψ_N at the mesh nodes and $\pi_N(\mathrm{Y})$ is the N-dimensional vector of the values of the function Y at the mesh points. Note that, by denoting with $\Psi_{N,i}$ the ith component, $i = 1, ..., N$, of the vector Ψ_N, eq 30 reads componentwise as the nonlinear algebraic system

$$\Psi_{N,i} = \mathcal{T}\left(\sum_{i=1}^{N} l_{N,j}(\theta_{N,i})\Psi_{N,j}\right),\ i = 1, ..., N$$

of N scalar equations in the N unknowns $\Psi_{N,i}$, where the functions $l_{N,j}$, $j = 1, ..., N$, are the Lagrange coefficients relevant to the nodes in Ω_N.

We use MATLAB software for the numerical computation. The discretized fixed point eq 29 is solved by the "fsolve" MATLAB function (present in the optimization toolbox), which finds solutions of systems of nonlinear algebraic scalar equations by a least-squares method.

The function "fsolve" requires the computation of values of the operator $\mathcal{F}$, and so, it requires the solution of the second order ordinary boundary value problems (eq 29). Such problems are restated as first-order equations and then solved by the "bvp4c" MATLAB function, which finds the solution of two-point ordinary boundary value problems by collocation. Finally, we remark that the integral in eq 29 is computed by the "quad" MATLAB function.

References and Notes

(1) Evans, D. F.; Wennerström, H. *The colloidal domain, where physics, chemistry, and biology meet*, 2nd ed.; VCH: New York, 1994.
(2) Bloomfield, V. A. *Biopolymers* **1997**, *44*, 269−282.
(3) DeRouchey, J.; Netz, R. R.; Rädler, J. O. *Eur. Phys. J. E* **2005**, *16*, 17−28.
(4) Xu, Z. P.; Zeng, Q. H.; Lu, G. Q.; Yu, A. B. *Chem. Eng. Sci.* **2006**, *61*, 1027−1040.
(5) May, S.; Ben-Shaul, A. *Curr. Med. Chem.* **2004**, *11*, 151−167.
(6) Boussif, O.; Lezoualch, F.; Zanta, M. A.; Mergny, M. D.; Scherman, D.; Demeneix, B.; Behr, J. P. *Proc. Natl. Acad. Sci. U.S.A.* **1995**, *92*, 7297−7301.
(7) Choosakoonkriang, S.; Lobo, B. A.; Koe, G. S.; Koe, J. G.; Middaugh, C. R. *J. Pharm. Sci.* **2003**, *92*, 1710−1722.
(8) Angelini, T. E.; Liang, H.; Wriggers, W.; Wong, G. C. L. *Proc. Natl. Acad. Sci. U.S.A.* **2003**, *100*, 8634−8637.
(9) Butler, J. C.; Angelini, T.; Tang, J. X.; Wong, G. C. L. *Phys. Rev. Lett.* **2003**, *91*, 028301/1-028301/4.
(10) Andelman, D. Electrostatic properties of membranes: The Poisson-Boltzmann theory. In *Structure and Dynamics of Membranes*, 2nd ed.; Lipowsky, R., Sackmann, E., Eds.; Elsevier: Amsterdam, 1995; Vol. 1.
(11) Neu, J. C. *Phys. Rev. Lett.* **1999**, *82*, 1072−1074.
(12) Kirkwood, J. G.; Shumaker, J. B. *Proc. Natl. Acad. Sci. U.S.A.* **1953**, *38*, 863−871.
(13) Oosawa, F. *Biopolymers* **1968**, *6*, 1633−1647.
(14) Guldbrand, L.; Joensson, B.; Wennerstroem, H.; Linse, P. *J. Chem. Phys.* **1984**, *80*, 2221−2228.
(15) Levin, Y. *Rep. Prog. Phys.* **2002**, *65*, 1577−1632.
(16) Grosberg, A. Y.; Nguyen, T. T; Shklovskii, B. I. *Rev. Mod. Phys.* **2002**, *74*, 329−345.
(17) Boroudjerdi, H.; Kim, Y. W.; Naji, A.; Netz, R. R.; Schlagberger, X.; Serr, A. *Phys. Rep.* **2005**, *416*, 129−199.
(18) Linse, P. *J. Phys.: Condens. Matter* **2002**, *14*, 13449−13467.
(19) Kjellander, R.; Marčelja, S.; Pashley, R. M.; Quirk, J. P. *J. Phys. Chem.* **1988**, *92*, 6489−6492.
(20) Kjellander, R.; Marčelja, S.; Pashley, R. M.; Quirk, J. P. *J. Chem. Phys.* **1990**, *92*, 4399−4407.
(21) Forsman, J. *Curr. Opin. Colloid Interface Sci.* **2006**, *11*, 290−294.
(22) Liu, X.; Yang, J. W.; Miller, A. D.; Nack, A. E.; Lynn, D. M. *Macromolecules* **2005**, *38*, 7907−7914.
(23) Claesson, P. M.; Poptoshev, E.; Blomberg, E.; Dedinaite, A. *Adv. Colloid Interface Sci.* **2005**, *114*−*115*, 173−187.
(24) Borukhov, I.; Andelman, D.; Orland, H. *Europhys. Lett.* **1995**, *32*, 499−504.
(25) Borukhov, I.; Andelman, D.; Orland, H. *J. Phys. Chem. B* **1999**, *103*, 5042−5057.
(26) Allen, R. J.; Warren, P. B. *Langmuir* **2004**, *20*, 1997−2009.
(27) Park, S. Y.; Bruinsma, R. F.; Gelbart, W. M. *Europhys. Lett.* **1999**, *46*, 454−460.
(28) Dobrynin, A. V.; Rubinstein, M. *Prog. Polym. Sci.* **2005**, *30*, 1049−1118.
(29) Huang, H.; Ruckenstein, E. *Adv. Colloid Interface Sci.* **2004**, *112*, 37−47.
(30) Podgornik, R.; Ličer, M. *Curr. Opin. Colloid Interface Sci.* **2006**, *11*, 273−279.
(31) Bohinc, K.; Iglič, A.; May, S. *Europhys. Lett.* **2004**, *68*, 494−500.
(32) Ohshima, H.; Ohki, S. *J. Coll. Int. Sci.* **1991**, *142*.
(33) Carnie, S.; McLaughlin, S. *Biophys. J.* **1983**, *44*, 325−332.
(34) Pianegonda, S.; Barosa, M.; Levin, Y. *Europhys. Lett.* **2005**, *71*, 831−837.
(35) Diehl, A.; Levin, Y. *J. Chem. Phys.* **2006**, *125*, 054902.
(36) Levin, Y. *J. Phys. Condens. Mater.* **2004**, *16*, S2149−S2152; Special Issue SI June 9, 2004.
(37) Linse, P. MOLSIM 4.1.7, Lund University, Sweden, 2006.
(38) Jönsson, B.; Wennerström, H.; Halle, B. *J. Phys. Chem.* **1980**, *84*, 2179−2185.
(39) Teif, V. B. *Biophys. J.* **2005**, *89*, 2574−2587.
(40) Hribar, B.; Vlachy, V. *J. Phys. Chem. B* **1997**, *101*, 3457−3459.